

CrI_3-WTe_2 : A Novel Two-Dimensional Heterostructure as Multisensor for BrF_3 and $COCl_2$ Toxic Gases.

Amreen Bano,¹ Jyoti Krishna,² T. Maitra,² and N. K. Gaur¹

¹Department of Physics, Barkatullah University, Bhopal-462026, India

²Department of Physics, Indian Institute of Technology Roorkee, Roorkee-247667, Uttarakhand, India

A new multisensor (i.e. resistive and magnetic) CrI_3-WTe_2 heterostructure (HS) to detect the toxic gases BrF_3 and $COCl_2$ (Phosgene) has been theoretically studied in our present investigation. The HS has demonstrated sensitivity towards both the gases by varying its electronic and magnetic properties when gas molecule interacts with the HS. Fast recovery time ($< 0.14fs$) under UV radiation has been observed. We have considered two configurations of BrF_3 adsorbed HS; 1) when F ion interacts with HS (C1) and 2) when Br ion interacts with HS (C2). In C1 case the adsorption energy E_{ad} is observed to be -0.66 eV while in C2 it is -0.95 eV. On the other hand in case of $COCl_2$ E_{ad} is found to be -0.42 eV. Magnetic moments of atoms are also found to vary upon gas adsorption indicates the suitability of the HS as a magnetic gas sensor. Our observations suggests the suitability of CrI_3-WTe_2 HS to respond detection of the toxic gases like BrF_3 and $COCl_2$.

I. INTRODUCTION

Gas detection for environmental monitoring has innumerable applications in field such as industries and agriculture, medical diagnosis, military etc.^{1,2} that utilizes the adsorption of gas molecules over materials. For the great technological perspective, it necessitates the material to have superior physical and chemical stability as well as the accessibility for chip-scale miniaturization of sensing elements for the low cost. Owing to the advent in 2D materials and increasing mass-market applications, the research in the gas sensors field have elevated rapidly due to continuing need for the highly sensitive, selective and faster response and recovery dynamics towards gas adsorption. The first 2D atomic crystal graphene has for a long time enticed because of its extraordinary mechanical and electronic properties. The desired requirement of high surface area, carrier mobility, chemical and thermal stability with low electronic temperature noise, power consumption and higher response time promises graphene to be used in the next generation devices employed in gas sensing and bio-sensing³⁻¹³. Since each atom in graphene is a surface atom, it results in the ultrasensitive sensor response. It has been seen that the epitaxially grown graphene based sensors are ultrasensitive towards NO_2 gas¹⁴. However, pristine graphene limits its potential upon physical adsorption of common gas molecules¹⁵⁻¹⁸ because of no dangling bonds. Thus for the chemisorptive enhancements, the surface is functionalized through polymers or metallic coating^{19,20}. Other forms of the graphene like graphene oxide (GO) or reduced GO do serve as a dynamic material for high performance molecular sensors²¹. Inspired by the performance of first 2D material, the gas sensing communities captured several hundreds of different 2D materials including elemental allotropes such as silicene, germanene borophene etc., and compound like transition metal dichalcogenides (TMDs)²². These have been tremendously successful in detecting even the traces of gas molecules like NO_2 , SO_2 , NH_3 etc.²³⁻²⁶. The forte

of these materials are their ability to engineer artificial heterostructures (HS). Because of the van der Waal interactions between the HS the lattice mismatching is not there that ultimately minimize the interfacial damages and chemical modification²⁷.

Recently the integration between magnetic layer and semiconductors initiate a new generation of advanced functional materials. By manipulating the exchange interactions the electronic structure in 2D materials can be altered²⁸⁻³⁰. Generally, the gas sensing mechanism is based on the principle of change in electronic properties with gas adsorption. Variation in magnetic properties upon gas adsorption has never been realized. We have investigated here the gas sensing ability of a magnetic HS with the magnetic CrI_3 integrated over WTe_2 monolayer upon interaction with noxious gases BrF_3 and phosgene ($COCl_2$). The BrF_3 a hazardous gas used mainly in processing of nuclear fuel. It is corrosive to metals and tissues and irritates the respiratory upon inhalation. On the otherhand, phosgene is highly toxic gas used in industries for production of pesticides and its immediate reaction starts even below 2-3 ppm. So far no investigation has been done on BrF_3 gas adsorption on sensor layer.

Thus this paper focusses on the study of how the gas molecules (BrF_3 and $COCl_2$) interfere with the electrical and magnetic properties upon interaction. We have also investigated the nature of adsorption and selectivity towards each gaseous molecules. Practically, a sensor's recovery time (R_T) is crucial for technological applications, thus R_T for the highly selective gas molecule is calculated for this system.

II. COMPUTATIONAL DETAILS

At ambient temperature and pressure conditions the crystal structure of CrI_3-WTe_2 HS is shown in Fig 1(a). The results presented here are obtained using first-principles approach which based on density func-

tional theory⁴¹ as implemented in Quantum Espresso package⁴². Ideally, CrI_3 exists in two crystal structures: 1) $AlCl_3$ type monoclinic array and 2) BiI_3 type rhombohedral order³¹. Here we report our findings for monoclinic assembly of CrI_3 deposited over hexagonal structure of WTe_2 ²⁷. In order to explore the electronic structure of pure and BrF_3 /Phosgene gas adsorbed CrI_3 - WTe_2 HS we have employed plane-wave ultrasoft pseudopotential method to trace the valence electron interactions. To serve the exchange-correlation potential, generalized gradient approximation (GGA) of Perdew-Burke-Erzerhof (PBE)⁴³ has been implemented. A supercell of $2 \times 2 \times 1$ has been used to construct CrI_3 - WTe_2 HS. The cut-off kinetic energy of 760 eV has been applied with $7 \times 7 \times 1$ K-mesh for Brillouin zones sampling. We have used these values after complete optimization process. To avoid any interaction among atomic orbitals we have provided a large vacuum of 17\AA along z direction. The CrI_3 - WTe_2 HS has been allowed to fully relax under the convergence of total energy and total forces which are found to be better than 1.0 meV. For gas sensing calculations, we have kept the structural geometry of CrI_3 - WTe_2 HS fixed and periodically moved the gas molecules BrF_3 and Phosgene $COCl_2$ (one at a time) along z direction in order to acquire the equilibrium distance d_{eq} between the HS and gas molecule. In case of BrF_3 gas molecule we have studied its interaction with the HS along two different orientations 1) F atom is interacting with HS surface and 2) Br atom is interacting with HS surface. The value of d_{eq} obtained in BrF_3 in case 1 is $\sim 2.25\text{\AA}$ whereas in case 2 it is observed to be $\sim 2.04\text{\AA}$. Moreover in case of Phosgene gas molecule d_{eq} is found within the range of $\sim 2.32\text{\AA}$ to $\sim 2.34\text{\AA}$. The adsorption energy of gas molecules BrF_3 (in both cases) and Phosgene adsorbed over CrI_3 - WTe_2 HS was defined as:

$$E_{ad} = E_{molecule/CrI_3-WTe_2HS} - E_{CrI_3-WTe_2HS} - E_{molecule} \quad (1)$$

where $E_{CrI_3-WTe_2HS}$ and $E_{molecule}$ indicates the total ground state energy of HS and gas molecule before adsorption take place respectively and $E_{molecule/CrI_3-WTe_2HS}$ shows the total ground state energy of gas molecule adsorbed HS.

III. RESULTS AND DISCUSSION

In the present investigation we have studied the HS which is comprised of monolayer of CrI_3 deposited over the honeycomb WTe_2 monolayer. Because of the presence of magnetic Cr^{3+} ion in CrI_3 layer of HS, we have first carried out calculation for two different magnetic configurations namely, ferromagnetic (FM) and antiferromagnetic (AFM) spin states at Cr site. Since the AFM state gives higher energy as compared to FM one, thus FM configuration is the stable magnetic state which is in accordance with the previous reports³¹. Hence, the fur-

TABLE I. Comparison of experimental and theoretically calculated bond length (\AA) of parent compounds WTe_2 and CrI_3 in HS. The bond lengths from theoretical structure is lesser as compared to experiments which shows an overall compression in the HS. The net compression is due to the formation of interfacial bonds among the Te and I ions upon optimization.

	Exp (\AA)	Calculations (\AA)
W-W ⁴⁰	3.6	3.2
W-Te ⁴⁰	2.769	1.448
Cr-Cr ³¹	3.96	2.16
I-I ³¹ (axis)	3.86	2.04
Cr-I ³¹	2.72	1.43

ther investigations have been done for FM configuration only.

A. Structural Analysis

The pristine HS shown in Fig 1(a) is composed of WTe_2 and CrI_3 monolayers. From Fig 1(a) we can see that in WTe_2 , the W ions forms a zig-zag pattern along a-axis resulting in slightly distorted hexagonal symmetry. The Te ions constitute an octahedral environment accompanied with strong intra-layer covalent bonding w.r.t W ions. Whereas, in the CrI_3 layer of HS, Cr^{3+} ions form a honeycomb lattice. The I- ions create an edge sharing octahedrally coordinated network w.r.t. Cr^{3+} ions such that the three I- ions are coordinated at the top and bottom layer of Cr ions. The two parent compounds (WTe_2 and CrI_3 monolayer) are vertically stacked together along c-axis to form a CrI_3 - WTe_2 HS with interfacial bonds linking I and Te ions. The $\langle Te - I \rangle$ average bond length at the interface is 2.61\AA . An overall compression along c-axis has also been observed among the parent compounds of the HS which may affect its electronic structure. Table 1. displays the comparison of experimental and calculated bond length in HS.

From the results obtained in Table 1 we observed a net compression in the HS (i.e. $< 45\%$) except for ($W - W$) ($\sim 11\%$) due to its relatively heavy atomic mass which obstructs any significant variation in its bond length as compared to other atoms. Hence the compression is emerging due to the interfacial bonds formed among the parent compounds of the HS (i.e. WTe_2 and CrI_3). These bonds are occurring from the charge transfer from Te ions to I ions (*charges flows from low electronegativity ($Te = 2.1$ Pauling scale) to high electronegativity ($I = 2.6$ Pauling scale)*). This process of bond formation at the interface of HS in turn results in compression of bond

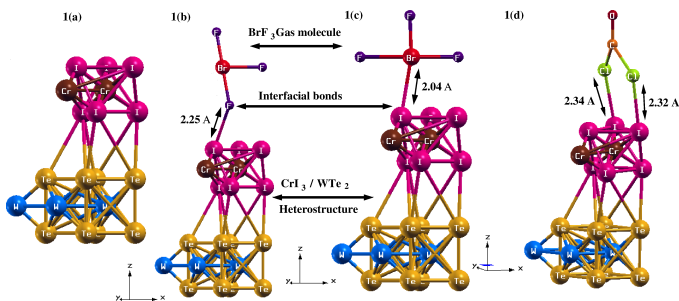


FIG. 1. Crystal structures of **a)** Pristine $CrI_3 - WTe_2$ HS showing interfacial bonds among the parent compounds i.e. CrI_3 and WTe_2 . These bonds results in net compression of the optimized HS. **b)** BrF_3 adsorbed $CrI_3 - WTe_2$ HS with C1 configuration when F ion is directly interacting with the surface of the HS with a separation of 2.25 Å. **c)** BrF_3 adsorbed $CrI_3 - WTe_2$ HS with C2 configuration when Br ion is directly interacting with the HS. The value of d_{eq} in this case has been observed to be 2.04 Å. **d)** $COCl_2$ adsorbed $CrI_3 - WTe_2$ HS with d_{eq} in range 2.32Å to 2.34Å. Only one configuration is considered for $COCl_2$ gas molecule due to larger reduced mass of Cl as compared to O ion.

length among the atoms upon optimization. The electronic properties of the HS may get influenced due to this compression which has been discussed in detail in the following section. The interaction of BrF_3 on HS can occur through two possible orientations: by forming an interfacial bond between (1) F and HS as shown in Fig 1(b) (C1 configuration), (2) Br and HS as shown in Fig 1(c) (C2 configuration). The $\langle F - Br - F \rangle$ bond angle is 86° with the $\langle Br - F \rangle$ bond length along axial and equatorial plane as 1.72 Å and 1.81 Å respectively. The equilibrium distance (d_{eq}) in C1 and C2 case is 2.25 Å and 2.04 Å respectively. For the $COCl_2$ gas the bond angle and bond length is 124° $\langle Cl - C - O \rangle$ and 1.76 Å $\langle Cl - C \rangle$, 1.19 Å $\langle C - O \rangle$ respectively. Unlike BrF_3 , only single orientation of $COCl_2$ has been considered (Cl linked with HS) as presented in Fig 1(d) due to larger reduced mass of Cl w.r.t O (about $\sim 10\%$) ions. The d_{eq} varies from 2.32-2.34 Å for this case.

B. Electronic Structure

In order to investigate the gas sensing effect of the HS, we have first studied the electronic density of states (DOS) prior to the gas adsorption. When no gas molecules were adsorbed, the total DOS of HS (Fig 2(a)) shows a spectral weight of 11.83 states/eV at Fermi level (FL). Small amount of metallicity is induced because of Cr-3d and I-5p orbitals of CrI_3 layer of HS. This induced metallicity is emerging from the compressed bond length of the atoms upon optimization as discussed above. Whereas the WTe_2 counterpart displays an insulating behaviour with a gap of 1.31 eV between majority and minority spin channels. Experimentally, CrI_3 layer

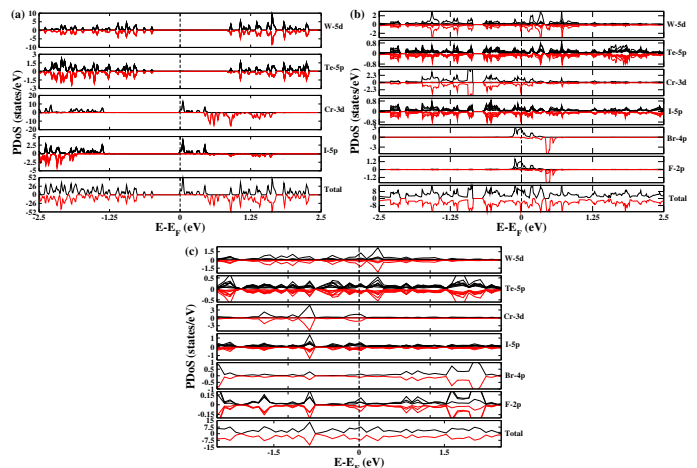


FIG. 2. Results of Partial density of states (PDoS) of **a)** Pristine $CrI_3 - WTe_2$ HS. The total DoS of HS showing half-metallic nature which is coming from the Cr^{3+} ions having vacant 3d states. W-5d states and Te-5p states of WTe_2 monolayer is showing an insulating character with clear band gap of 1.31 eV. **b)** C1 of BrF_3 adsorbed HS. It is evident from the result that in C1 configuration the HS has become a metal unlike pristine HS which is a half-metal. On the other hand the spin-up states of the gas molecule BrF_3 is actively contributing in the metallicity of the HS while spin-down states are present around 0.58 eV in the conduction band region. **c)** C2 configuration of BrF_3 adsorbed HS. It can be seen that when Br ion interacts with HS there is no spin splitting exists among both spin channels unlike the C1 case.

is insulating in nature³¹ but in CrI_3-WTe_2 HS, half-metallicity is observed. This might be due to the electron doping of CrI_3 layer induced by WTe_2 as reported previously³². Near FL ($E = -0.48$ eV) only contributions from W-5d orbital and Te-5p orbital dominates whereas Cr-3d and I-5p orbital state lies 1.32 eV below FL. For pristine HS the total bandwidth for metallic state is observed to be 0.02 eV (Fig 2(a)) with the majority spin carriers separated from minority spin carriers by 0.88 eV.

1) BrF_3 Adsorbed HS:

When BrF_3 gas molecule is adsorbed on the HS the metallicity is enhanced in both the orientations which can be seen from Fig 2(b) and Fig 2(c). In C1 configuration (Fig 2(b)), when F directly forms an interfacial bonding with HS, the bandwidth increases to 0.67 eV. At FL, the dominant contribution is coming from Cr-3d states with the spectral weight for up and down spin density being 0.85 states/eV and 1.56 states/eV respectively. Feeble participation of W-5d (up 0.33 states/eV, down 0.77 states/eV) and Te-5p (up 0.14 states/eV, down 0.21 states/eV) and I-5p states (up 0.23 states/eV, down 0.37 states/eV) are also observed at FL. The adsorbed BrF_3 gas molecule in C1 have enhanced spin up DOS at FL.

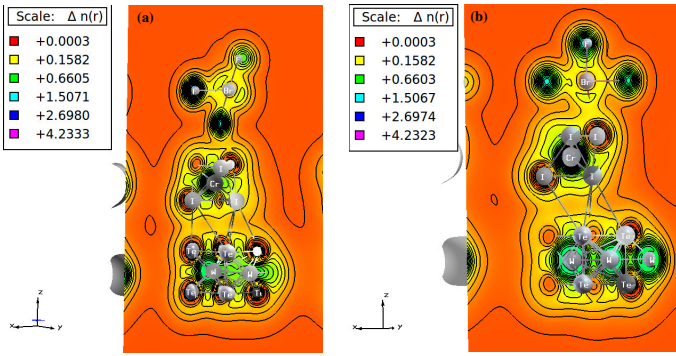


FIG. 3. The charge density results of **a)** C1 configuration of BrF_3 adsorbed HS showing the charge transfer network among the HS and gas molecule. This also confirms the presence of chemisorptive nature of bond which has influenced the electronic structure of pristine HS. **b)** C2 configuration of BrF_3 adsorbed HS. The charges are appeared to flow from I ions to the gas molecule. Among all the atomic species present in the HS and the gas molecule, maximum electronegativity is possessed by F ions hence charges will get accumulate at F ions site.

In principle, the charges should flow from Br (low electronegativity) to F (high electronegativity) ions but due to the large $\langle Br - F \rangle$ bond length ($< 1.7 \text{ \AA}$) the charge hopping takes place at slower rate resulting in higher spectral weight of Br (2.08 states/eV) ion as compared to F (0.97 states/eV) ions at FL. On the other side for C2 configuration (Fig 2(c)), when Br interacts directly with HS, the bandwidth further intensifies to 0.76 eV at FL. Likewise in C1, here also the Cr-3d states are pronounced at FL with spectral weight of 1.25 states/eV for all spin channels. Relatively weak involvement of W-5d (0.95 states/eV), Te-5p (0.2 states/eV) and I-5p (0.42 states/eV) states are present at FL. Now since the electronegativity of I, Br and F are 2.66, 2.96 and 3.98 Pauling scale respectively, therefore a continuous flow of the charge will take place from I to F via Br ion. Hence, net charge density at Br site decreases as compared to previous case. In C2, the net charge transport takes place through I-Br-F chain which facilitates the smooth transfer without any accumulation while the charges stocked at Br site due to uneven path (I-F-Br) w.r.t. electronegativity in C1. To investigate the nature of bonding between BrF_3 and HS, we have studied the charge density for both the orientations (Fig 3(a) and Fig 3(b)). For this purpose the calculations were performed in (1 1 0) plane. As discussed earlier that the charge transport channel is decided by the electronegativity difference. In C1 (Fig 3(a)), electronegativity of WTe_2 , CrI_3 and BrF_3 is 1.5071, 2.6980 and 4.2333 respectively where the maximum charge is accumulated near F (4.2333) ion of BrF_3 . Hence, a net flow of charge will take place from WTe_2 to BrF_3 layer via CrI_3 . Similar charge flow network is followed in C2 as shown in Fig 3(b) where electronegativity of WTe_2 , CrI_3 and BrF_3 is observed to be 1.5067, 2.6974 and 4.2323.

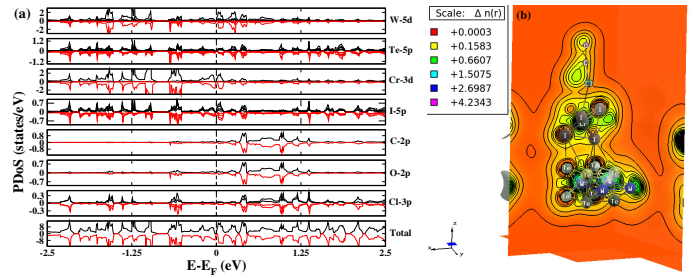


FIG. 4. **a)** PDOS of $COCl_2$ adsorbed HS showing a 'gapless' type semiconducting behaviour. The term gapless is justified by the fact that the electronic states of HS species are not overlapped at the Fermi level. The energy states of gas molecule $COCl_2$ shows no significant contribution near Fermi level. **b)** The charge density result of Phosgene gas molecule adsorbed over HS indicates a unidirectional charge flow from HS to the gas molecule which causes the charge accumulation at $COCl_2$. O ion is most electronegative in this case hence charges will be gathered at O ion site.

2) Phosgene ($COCl_2$) Adsorbed HS:

Another poisonous gas $COCl_2$ when adsorbed on the HS surface exhibits a gapless type semiconducting behaviour which can be seen in Fig 4(a) showing the PDOS of the above stated system. With adsorption the states are present near the FL but does not crosses for W and Te ions. Similar situation is observed for Cr-3d and I-5d states. This is in contrast with BrF_3 adsorption where the metallicity was induced at each HS layer. Within -0.26 eV-0.31 eV energy window, the HS is occupied by the states of both spin channels near FL whereas, negligible contributions are coming from the gaseous states in that energy range. In the $COCl_2$ gas molecule, the electronegativity of C, Cl and O are 2.55, 3.16 and 3.44 Pauling scale respectively. Thus, the charge flow from C will take place to O and Cl ions resulting in slight occupation of states below FL in O and comparatively higher states at Cl site. The DOS of Cl ions (Fig 4(a)) has the 3p states peaked within 0.5 eV - 0.7 eV below FL due to higher charge density coming from C and HS layers. From the charge density calculations we observed a charge flow direction from HS to the gas molecule as given in Fig 4(b). The electronegativity of WTe_2 , CrI_3 and $COCl_2$ is 1.5075, 2.6987, 4.2343 respectively. It results in a unidirectional charge flow from bottom of HS to the gas molecule which causes the accumulation of carriers at $COCl_2$. The above observations suggest that CrI_3 - WTe_2 HS serve as a potential gas sensor for BrF_3 and $COCl_2$ gas molecule.

C. Magnetic Properties

In HS the magnetic contribution is coming due CrI_3 layer which has FM ordering with total spin magnetic moment of $5.35 \mu_B$. And the magnetic moment per Cr

and I ions are $2.86 \mu_B$ and $0.041 \mu_B$ respectively. This is in good agreement with the saturation moment ($3.1 \mu_B/\text{Cr}$) measured experimentally³¹. The low magnetic moment of I ions is due to the transfer of unpaired 4s electron from Cr to I- resulting in stable 5p states. This delocalization of charges causes reduced moment at I-site. On the other hand, the $WT e_2$ layer in HS remains non-magnetic. With the exposure of BrF_3 gas molecule in C1 configuration, the delocalization effects dominate in Cr ions resulting in decreased magnetic moment. The Br and F ions on the other hand acquire charges from HS have higher mag moment ($0.088 \mu_B$ for Br and $0.005 \mu_B$, $0.144 \mu_B$, $0.0268 \mu_B$ per F ion) as compared to Cr^{3+} ($0.009 \mu_B$). As discussed above that due to difference in $\langle Br - F \rangle$ bond lengths uneven charge flow takes places to form dissimilar magnetic moment per F ion. In C2 configuration when Br directly bonded with HS layer total magnetic moment is almost negligible. This is in accordance with the DOS of C2 (Fig 2(c)) where the net reduction in spectral weight was observed. Due to the continuous charge transfer path (I-Br-F) the delocalization of electrons causes the moments to drop. The same scenario has been observed when Phosgene is exposed to HS. The overall reduction in magnetic moment is observed here as well. The variation in magnetic moments of the HS upon interaction of gas molecules suggests that CrI_3-WTe_2 HS can be used as a magnetic gas sensor as well as resistive gas sensor. There are many studies over the latter type but only few experimental studies are performed on the former type of gas sensor which detects the perturbation in the magnetic properties when gas molecules interact with the sensor material³³. A few magnetic gas sensors so far studied are nanoparticles of $CuFe_2O_4$ which was used for the detection of volatile organic compounds (VOCs)³⁴, Co/ZnO nanorods to detect H_2 and CO molecules³⁵, Co/ZnO hybrid nanostructures for the detection of C_3H_6O , CO and H_2 target gases³⁶ etc.

D. Adsorbtion and recovery time

The adsorbtion energy describes the nature of stability among adsorbent (HS) and adsorbate (gas molecule). The process can take place in two modes (1) physisorption: which involves weak van der Waals forces between two reacting species. The electronic properties of adsorbent is barely perturbed during this mechanism; (2) chemisorption: here actual involvement of chemical bonds between species exists. This also require minimum activation energy to initiate the process. In C1 with BrF_3 adsorption on HS, the adsorption energy is -0.66 eV while in C2 it increases to -0.95 eV. The increasing adsorption rate by 30% suggests the comparatively strong chemisorptive nature in C2. The existence of strong covalent bonding between HS and BrF_3 (C1 and C2) have been observed from charge density results shown in Fig 3(a) and Fig 3(b). Similar studies for $COCl_2$ adsorption

TABLE II. Adsorbtion energy ($E_{ad}(eV)$) and recovery time R_T (fs) for BrF_3 and $COCl_2$ gas adsorption over HS layer. In the I coloumn, the E_{ad} of BrF_3 and $COCl_2$ gases showing chemisorptive nature. The highest E_{ad} in BrF_3 represents the strongest covalent bonding between the gas molecule and HS. From the II, III and IV coloumns, the recovery is fastest when the sensor is illuminated with UV radiation.

	$E_{ad}(eV)$	R_T (IR) (fs)	R_T (Visible) (fs)	R_T (UV) (fs)
BrF_3 (C1)	-0.66	1302	13.02	0.13
BrF_3 (C2)	-0.95	1460	14.6	0.14
$COCl_2$	-0.42	1180	11.8	0.12

shows the chemisorptive character but the E_{ad} (-0.42 eV) is relatively smaller than that from BrF_3 interaction. It is evident that as d_{eq} increases, E_{ad} energy decreases. Thus, the higher d_{eq} for $COCl_2$ case is marked by decrease in E_{ad} . Though the relative stability in $COCl_2$ case is lesser than BrF_3 but from previous literature $COCl_2$ adsorption on BN nano tube (BNNT), BN nano rod (BNNR) and borophene reported to have E_{ad} -0.18 eV, -1.058 eV and -0.306 eV respectively^{37,38}. Hence, $COCl_2$ adsorption on CrI_3-WTe_2 HS has shown better performance as compared to previous reports with an exception of BNNR.

The recovery time R_T of a sensor is based on how fast the sensor retrieve its initial state. Based on the Arrhenius theory the sensor recovery time³⁹ is related by:

$$R_T = \nu^{-1} e^{-E_{ad}/KT} \quad (2)$$

where, ν is the operational frequency, E_{ad} is adsorbate energy, K is Boltzmann constant and T is the sensor's operational temperature. For different attempt frequencies, the sensor's recovery rate is affected as tabulated in Table 2. Under UV illumination the HS is showing faster R_T for all the cases. The recovery rate depends on the nature of adsorption. With relatively weak chemisorptive effect of $COCl_2$ gas on HS, fastest recovery time is achieved.

IV. CONCLUSIONS

We have theoretically investigated a new 2-dimensional CrI_3-WTe_2 HS in the present work in order to explore the possibility as a multisensor (i.e. resistive and magnetic). Our results shows that upon interaction with the gas molecules BrF_3 and $COCl_2$ with HS the electronic as well as magnetic properties of pristine HS get altered. We have also determined that how swiftly the HS can get recover after detaching the gaseous species from it by means of recovery time. We found that under UV illumination ultrafast recovery time is presented by the HS i.e. $< 0.14fs$. Hence we conclude that CrI_3-WTe_2 HS

offers it self as a multisensor for the detection of highly toxic gases like BrF_3 and $COCl_2$.

- ¹ Yang, S., Jiang, C. & Wei, S-h. Gas sensing in 2D materials. *Appl. Phys. Rev.* **4**, 021304 (2017).
- ² Kuchyanov, A. S., Chubakov, P. A., Spisser, H. & Plekhanov, A. I. Highly sensitive and fast response gas sensor based on a light reflection at the glass-photonic crystal interface. *Opt. Commun.* **351**, 109-114 (2015).
- ³ Neto, A. H. C., Guinea, F., Peres, N. M., Novoselov, K. S. & Geim, A. K. The electronic properties of graphene. *Rev. Mod. Phys.* **81**, 109 (2009).
- ⁴ Balandin, A. A., Ghosh, S., Bao, W., Calizo, I, Teweldebrhan, D., Miao, F. & Lau, C. N. Superior thermal conductivity of single-layer graphene. *Nano Lett.* **8**, 902 (2008).
- ⁵ Nobakht, A. Y., Shin, S., Kihm, K. D., Marable, D.C. & Lee, W. Heat flow diversion in supported graphene nanomesh. *Carbon* **123**, 45-53 (2017).
- ⁶ Nobakht, A. Y. & Shin, S. Anisotropic control of thermal transport in graphene/Si heterostructures. *J. Appl. Phys.* **120**, 225111 (2016).
- ⁷ Basu, S. & Bhattacharyya, P. Recent developments on graphene and graphene oxide based solid state gas sensors. *Sens. Actuators B-Chem.* **173**, 1-21 (2012).
- ⁸ He, Q., Wu, S., Yin, Z. & Zhang, H. Graphene-based electronic sensors. *Chem. Sci.* **3**, 1764-1772 (2012).
- ⁹ Pumera, M. Graphene in biosensing. *Mater. Today* **14**, 308-315 (2011).
- ¹⁰ Fowler, J. D., Allen, M. J., Tung, V. C., Yang, Y., Kaner, R. B. & Weiller, B. H. Practical chemical sensors from chemically derived graphene. *ACS Nano* **3**, 301-306 (2009).
- ¹¹ Ko, G., Kim, H.-Y., Ahn, J., Park, Y.-M., Lee, K.-Y. & Kim, J. Graphene-based nitrogen dioxide gas sensors. *Curr. Appl. Phys.* **10**, 1002-1004 (2010).
- ¹² Chen, G., Paronyan, T. M. & Harutyunyan, A. R. Sub-ppt gas detection with pristine graphene. *Appl. Phys. Lett.* **101**, 053119 (2012).
- ¹³ Sabury, S., Kazemi, S. H. & Sharif, F. Graphene-gold nanoparticle composite: Application as a good scaffold for construction of glucose oxidase biosensor. *Mater. Sci. Eng. C* **49**, 297-304 (2015).
- ¹⁴ Pearce, R., Iakimov, T., Andersson, M., Hultman, L., Spetz, A. L. & Yakimova, R. Epitaxially grown graphene based gas sensors for ultrasensitive NO_2 detection. *Sens. Actuators B-Chem.* **155**, 451-455 (2011).
- ¹⁵ Robinson, J. T., Perkins, F. K., Snow, E. S., Wei, Z. & Sheehan, P. E. Reduced graphene oxide molecular sensors. *Nano Lett.* **8**, 3137-3140 (2008).
- ¹⁶ Zhang, Y. H., Chen, Y. B., Zhou, K. G., Liu, C. H., Zeng, J., Zhang, H. L. & Peng, Y. Improving gas sensing properties of graphene by introducing dopants and defects: a first-principles study. *Nanotechnology* **20**, 185504 (2009).
- ¹⁷ Lu, G., Ocola, L. E. & Chen, J. Reduced graphene oxide for room-temperature gas sensors. *Nanotechnology* **20**, 445502 (2009).
- ¹⁸ Arsat, R., Breedon, M., Shafiei, M., Spizziri, P. G., Gilje, S., Kaner, R.B., Kalantarzadeh, K. & Wlodarski, W. Graphene-like nano-sheets for surface acoustic wave gas sensor applications. *Chem. Phys. Lett.* **467**, 344-347 (2009).
- ¹⁹ Lang, B. A leed study of the deposition of carbon on platinum crystal surfaces. *Surf. Sci.* **53**, 317-329 (1975).
- ²⁰ Pumera, M., Ambrosi, A., Bonanni, A., Chng, E. L. K. & Poh, H. L. Graphene for electrochemical sensing and biosensing. *Trends Anal. Chem.* **29**, 954-965 (2010).
- ²¹ Schedin, F., Geim, A. K., Morozov, S. V., Hill, E. W., Blake, P., Katsnelson, M. I. & Novoselov, K. S. Detection of individual gas molecules adsorbed on graphene. *Nat. Mater.* **6**, 652-655 (2007).
- ²² Miró, P., Audiffred, M. & Heine, T. An atlas of two-dimensional materials. *Chem. Soc. Rev.* **43**, 6537-6554 (2014).
- ²³ Hu, W., Xia, N., Wu, X., Li, Z. & Yang, J. Silicene as a highly sensitive molecule sensor for NH_3 , NO and NO_2 . *Phys. Chem. Chem. Phys.* **16**, 6957-6962 (2014).
- ²⁴ Cho, B., Hahm, M. G., Choi, M., Yoon, J., Kim, A. R., Lee, Y. -J., Park, S. -G., Kwon, J. -D., Kim, C. S., Song, M., Jeong, Y., Nam, K. -S., Lee, S., Yoo, T. J., Kang, C. G., Lee, B. H., Ko, H. C., Ajayan, P. M. & Kim, D. -H. Charge-transfer-based gas sensing using atomic-layer MoS_2 . *Sci. Rep.* **5**, 8052 (2015).
- ²⁵ Kou, L., Fraunheim, T. & Chen, C. Phosphorene as a superior gas sensor: selective adsorption and distinct I-V response. *J. Phys. Chem. Lett.* **5**, 2675-2681 (2014).
- ²⁶ He, Q., Zeng, Z., Yin, Z., Li, H., Wu, S., Huang, X. & Zhang, H. Fabrication of flexible MoS_2 thin-film transistor arrays for practical gas-sensing applications. *Small* **8**, 2994 (2012).
- ²⁷ Zhong, D., Seyler, K. L., Linpeng, X., Cheng, R., Sivadas, N., Huang, B., Schmidgall, E., Taniguchi, T., Watanabe, K., McGuire, M. A., Yao, W., Xiao, D., Fu, K. -M. C. & Xu, X. Van der Waals engineering of ferromagnetic semiconductor heterostructures for spin and valleytronics. *Sci. Adv.* **3**, 5 (2017).
- ²⁸ Haugen, H., Huertas-Hernando, D. & Brataas, A. Spin transport in proximity-induced ferromagnetic graphene. *Phys. Rev. B* **77**, 115406 (2008).
- ²⁹ Qiao, Z., Yang, S. A., Feng, W., Tse, W. -K., Ding, J., Yao, Y., Wang, J. & Niu, Q. Quantum anomalous Hall effect in graphene from Rashba and exchange effects. *Phys. Rev. B* **82**, 161414(R) (2010).
- ³⁰ Korenev, V. L., Salewski, M., Akimov, I. A., Sapega, V. F., Langer, L., Kalitukha, I. V., Debus, J., Dzhioev, R. I., Yakovlev, D. R., Müller, D., Schröder, C., Hövel, H., Karczewski, G., Wiater, M., Wojtowicz, T., Kusrayev, Y. G. & Bayer, M. Long-range p-d exchange interaction in a ferromagnet-semiconductor hybrid structure. *Nat. Phys.* **12**, 85-91 (2016).
- ³¹ McGuire, M. A., Dixit, H., Cooper, V. R. & Sales, B. C. Correction to Coupling of Crystal Structure and Magnetism in the Layered, Ferromagnetic Insulator CrI_3 . *Chem. Mater.* **27**, 612-620 (2015).
- ³² Wang, H., F. Fan., Zhu, S. & Wu, H. Doping enhanced ferromagnetism and induced half-metallicity in CrI_3 monolayer. *Europhys. Lett.* **114**, 47001 (2016).
- ³³ Punnoose, A., Reddy, K. M., Thurber, A., Hays, J. & Engelhard, M. H. Novel magnetic hydrogen sensing: a case study using antiferromagnetic haematite nanoparti-

- cles. *Nanotechnology* **18**, 165502 (2007).
- ³⁴ Matatagui, D., Kolokoltsev, O. V., Qureshi, N., Mejia-Uriarte, E. V. & Saniger, J. M. A magnonic gas sensor based on magnetic nanoparticles. *Nanoscale* **7**, 9607-9613 (2015).
- ³⁵ Ponzoni, A., Baratto, C., Cattabiani, N., Falasconi, M., Galstyan, V., Carmona, E. N., Rigoni, F., Sberveglieri, V., Zambotti, G. & Zappa, D. Metal oxide gas sensors, a survey of selectivity issues addressed at the SENSOR Lab, Brescia (Italy). *Sensors* **17**, 714 (2017).
- ³⁶ Ciprian, R., Torelli, P., Giglia, A., Gobaut, B., Ressel, B., Vinai, G., Stupar, A. C., Ninno, G. D., Pincelli, T., Casarin, G., Sberveglieri, G., Baratto, C. & Malvestuto, M. New strategy for magnetic gas sensing. *RSC Adv.* **6**, 83399-83405 (2016).
- ³⁷ Beheshtiana, J., Peyghanb, A. A. & Bagheric, Z. Detection of phosgene by Sc doped BN nanotubes: a DFT study. *Sens. Actuators B-Chem.* **171**, 846-852 (2012).
- ³⁸ Patel, K., Roondhe, B., Dabhi, S. D. & Jha, P. K. A new flatland buddy as toxic gas scavenger: A first principles study. *J. Hazard. Mater.* **351**, 337-345 (2018).
- ³⁹ Pitt, G. I., Gilbert, R. G. & Ryan, K. R. Application of transition-state theory to gas surface reactions: barrier less adsorption on clean surfaces. *J. Phys. Chem.* **98**, 13001-13010 (1994).
- ⁴⁰ Lee, C. -H., Silva, E. C., Calderin, L., Nguyen, M. A. T. , Hollander, M. J., Bersch, B., Mallouk, T. E. & Robinson, J. A. Tungsten ditelluride: a layered semimetal. *Sci. Rep.* **5**, 10013 (2015).
- ⁴¹ Hohenberg, P. & Kohn, W. Inhomogeneous electron gas. *Phys. Rev.* **136**, B864 (1964).
- ⁴² Giannozzi, P., Baroni, S., Bonini, N., Calandra, M., Car, R., Cavazzoni, C., Ceresoli, D., Chiarotti, D. L., Cococcioni, M., Dabo, I., Dal Corso, A., Fabris, S., Fratesi, G., Gironcoli, S. de, Gebauer, R., Gerstmann, U., Gougoussis, C., Kokalj, A., Lazzeri, M., Martin-Samos, L., Marzari, N., Mauri, F., Mazzarello, R., Paolini, S., Pasquarello, A., Paulatto, L., Sbraccia, C., Scandolo, S., Sclauzero, G., Seitsonen, A. P., Smogunov, A., Umari, P. & Wentzcovitch, R. M. QUANTUM ESPRESSO: a modular and open-source software project for quantum simulations of materials. *J. Phys.: Condens. Matter* **21**, 395502 (2009).
- ⁴³ Perdew, J. P., Burke, K. & Ernzerhof, M. Generalized gradient approximation made simple. *Phys. Rev. Lett.* **77**, 3865 (1996).